JMEPEG (2020) 29:8431–8440
https://doi.org/10.1007/s11665-020-05302-x

1059-9495/$19.00

Effects of Cl^- and AC on the Corrosion Behavior of 2507 Super Duplex Stainless Steel in a Simulated Concrete Pore Solution

M. Zhu, Q. Zhang, Y.F. Yuan, S.Y. Guo, and J. Pan

Submitted: 30 July 2020 / Revised: 7 October 2020 / Accepted: 18 October 2020 / Published online: 17 November 2020

The effects of Cl^- concentration and applied alternating current (AC) on the corrosion behavior of 2507 super duplex stainless steel (SDSS) were studied in a saturated $Ca(OH)_2$ solution by electrochemical measurements, immersion test, and x-ray photoelectron spectroscopy. The results show that the presence of Cl^- ions accelerates the corrosion of 2507 SDSS in the saturated $Ca(OH)_2$ solution. The protective ability of passive film decreases as Cl^- concentration increases, especially at the concentration of 10% Cl^-. As the applied i_{AC} increases, the i_p value increases, and the E_p value decreases. The applied AC increases the number of defects within the passive film, affects the electronic property of the surface film, which results in a harmful effect on the passive film, and weakens its anti-corrosion property. The higher the i_{AC}, the more severe the damage influence is. Moreover, imposed AC promotes the pitting corrosion sensitivity of SDSS and enhances its corrosion rate. The applied AC and the addition of Cl^- exert a combined effect, reducing the corrosion resistance of passive film formed on 2507 SDSS.

Keywords 2507 SDSS, AC interference, corrosion behavior, passive film

1. Introduction

In recent years, AC interference has accelerated the corrosion of metallic materials employed in some industries. Many researchers have studied the related works (Ref 1-3). Jiang (Ref 4) reported that Tafel slope determined the change trend of offset direction of corrosion potential of Q235 steel. Tang et al. (Ref 5) concluded that AC interference affected the cathodic current provided by magnesium, causing a decreased protection effect for pipeline steel. Fu (Ref 6) reported that uniform corrosion occurred on X65 steel at lower i_{AC}, whereas pit corrosion was found at higher current density. Wen (Ref 7) indicated that the applied AC current density could greatly affect the number of pits formed on steel. Wan (Ref 8) proposed that AC could facilitate the organic matter transfers and enhance the corrosion of X80 steel. Additionally, Bacillus cereus enhanced the occurrence of pitting and increased the stress corrosion cracking (SCC) susceptibility of API 5L the steel. Wang (Ref 9) found that imposed AC increased the SCC susceptibility of pipeline steel under cathodic protection (CP) conditions. Our recent studies (Ref 10-12) indicated that applied AC caused a change in the SCC behavior and mechanism, and the AC corrosion behavior of pipeline steel in a slightly alkaline environment was related with the microstructure (Ref 13). To date, the relevant reports on AC corrosion are concentrated on pipeline steels in soil environments (Ref 14-16).

It is well known that the reinforced concrete structure possesses excellent protective ability due to the formation of protective film layer when in highly alkaline environment. At present, increasing stainless steels as rebar have been widely used in concrete structures because of their good comprehensive performances, including good corrosion resistance, high mechanical properties and long service life (Ref 17-19). A number of researchers have reported corrosion status of rebars in simulated concrete environments (Ref 20-24). Luo (Ref 25) reported that an increase in the Cr/Fe ratio within the passive film could promote the pitting corrosion resistance of AISI 316 stainless steel. Alonso (Ref 26) found that Ni could affect the corrosion resistance of duplex stainless steel (DSS) in a solution with Cl^- ions to some extent. Briz (Ref 27) indicated that 2001 lean duplex stainless steel (LDSS) exhibited a higher stress corrosion cracking (SCC) sensitivity than that of 2205 DSS in a concrete pore solution containing chloride. Moser (Ref 28) proposed that when the concentration of Cl^- ions was less than 0.5 M, the stainless steels of UNS S32304 and S32205 had a high anti-stress corrosion cracking property. Due to its excellent corrosion resistance in the environments containing Cl^- ions (Ref 29, 30), 2507 SDSS is widely used in the structural applications of many industries. However, the report about the corrosion behavior of 2507 SDSS employed in the simulated concrete pore solution with pH value of about 12.5 (Ref 31) is rare. Our previous research indicated that the difference in the protective capability of primary and secondary passive films formed on 2507 SDSS in a simulated concrete pore solution was attributed to their structure and composition.

In offshore marine engineering and seashore areas near super-high voltage transmission lines, AC interference is frequently detected (Ref 14, 32, 33). When 2507 SDSS served as rebar in concrete structures near AC electric field, the passive

M. Zhu, College of Materials and Chemistry, China Jiliang University, Hangzhou 310018, China; and School of Mechanical Engineering and Automation, Zhejiang Sci-Tech University, Hangzhou 310018, China; and **Q. Zhang, Y.F. Yuan, S.Y. Guo,** and **J. Pan**, School of Mechanical Engineering and Automation, Zhejiang Sci-Tech University, Hangzhou 310018, China. Contact e-mail: zmii2009@163.com.

film with outstanding corrosion resistance may be destroyed, which may accelerate the corrosion failure of SDSS rebar in concrete structure used in offshore marine engineering. Nevertheless, there is no literature regarding the effect of AC on the corrosion behavior of SDSS acted as a rebar material in simulated concrete pore solution.

In this work, the corrosion behavior of 2507 SDSS interfered by AC in simulated concrete pore solution containing Cl^- was investigated by electrochemical measurements, immersion test and x-ray photoelectron spectroscopy (XPS). These research results can provide a necessary reference for the related engineering applications.

2. Experimental

2.1 Material and Solution

In this work, a commercial SAF2507 SDSS is adopted and provided in the form of hot-rolled, with the solution-annealed status. Its chemical composition (wt.%) is C 0.018, Si 0.47, Mn 0.75, P 0.023, S 0.001, Cr 25, Ni 6.92, Mo 3.89, N 0.269 and Fe balance. Figure 1 shows the microstructure of 2507 SDSS. It is composed of austenite phase (γ) and ferrite phase (α), and a part of α are embed within γ. The samples with dimension of 10 mm × 10 mm × 5 mm were packaged with epoxy resin, leaving an exposed region of 1 cm^2. Subsequently, the specimen was ground, polished, rinsed and air-dried. A saturated $Ca(OH)_2$ solution with a pH of 12.6 was used to simulate the concrete environment (Ref 34-36). The addition of various Cl^- concentrations (0, 1, 3, 5, 10 wt.%) in the simulated concrete pore solution was done to study the influence of Cl^- on the corrosion behavior of 2507 SDSS as potential rebar. The Cl^- concentrations were achieved by adding sodium chloride salt. All tests were performed at a constant temperature of 25 °C.

2.2 Electrochemical Tests

Without the applied AC, the electrochemical measurements were conducted at PARSTAT2273 electrochemical workstation with a conventional three-electrode cell system. Among them, the SDSS sample was acted as the working electrode, a Pt plate as the counter electrode, and a saturated calomel electrode (SCE) as the reference electrode. The polarization curves of the specimens in the saturated $Ca(OH)_2$ solution containing different Cl^- concentrations were measured in a potential range of − 1.2 V (vs. SCE) to 1.2 V (vs. SCE) with a sweep rate of 0.5 mV/s.

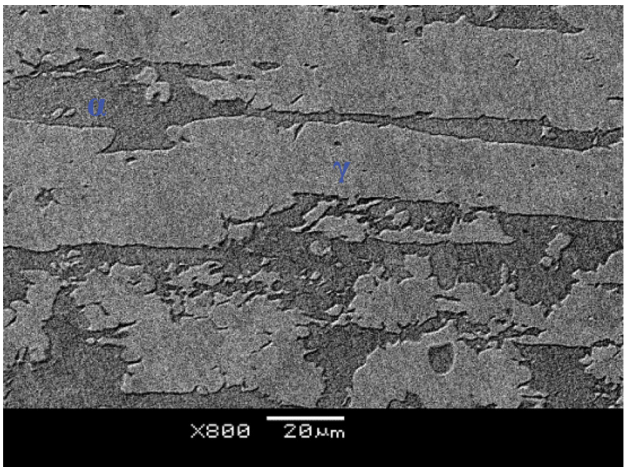

Fig. 1 Microstructure of 2507 SDSS

In the presence of imposed AC, the electrochemical tests of SDSS sample were performed at various AC current densities (i_{AC}) of 0, 50, 100 and 200 A/m^2 in the saturated $Ca(OH)_2$ solution with 3.5 wt.% NaCl. The Cl^- concentration was selected to simulate the salinity of ocean water. The set parameters of polarization curve were identical to those in the absence of AC interference. The testing setup of the electrochemical curve of SDSS sample with applied AC was in accordance with our previous literature (Ref 10, 37). A 50 Hz sinusoidal AC was applied during the testing process.

To investigate the effect of applied AC on the passive film formed on the surface of SDSS, the film was generated at an anodic potential of 0.42 V for 1 h using the potentiostatic polarization method, and then the formed film was interfered at different i_{AC} for 5 min, finally the electrochemical impedance spectroscopy (EIS) and Mott–Schottky curves were adopted to measure the influence of the applied AC. EIS curve was performed from 100 kHz to 10 mHz at open-circuit potential with an applied interfering signal amplitude of 10 mV. Afterwards, Mott–Schottky curve was measured at a fixed frequency of 1 kHz from − 1.0 to 1.0 V with a step size of 50 mV. The above measurements were repeated at least three times.

2.3 Immersion Test

The superimposed AC circuit in the above testing setup was adopted to conduct the immersion test. The sample used in the test was the same as that employed in the electrochemical tests. Before the test, the sample was washed, dried and weighed. Then, the specimens exposed to various i_{AC} of 0, 50 and 100 A/m^2 were immersed into the saturated $Ca(OH)_2$ solution containing 3.5 wt.% Cl^- for 10 days. After the experiment, the rusts formed on the surface of SDSS sample were completely removed by a 10 vol.% nitric acid solution. Subsequently, the specimen was successively rinsed, dried, and weighed. Then, the average corrosion rates of SDSS samples interfered at different i_{AC} were calculated by the weight loss, and the corrosion morphologies were analyzed by SEM. The test was repeated at least three times.

2.4 XPS Analysis

X-ray photoelectron spectroscopy (XPS) (Thermo Fisher Scientific, USA) was used to analyze the composition of passive films formed on SDSS samples under three testing conditions.

The first and second conditions are as follows: the passive films were grown on the surface of SDSS at a constant anodic potential of 0.42 V for 1 h in saturated $Ca(OH)_2$ solution without or with 3.5 wt.% Cl^-. The third case is below: AC of 100 A/m^2 was applied to interfere the film formed under the second case for 5 min. Then, the SDSS samples covered with three kinds of passive films were transferred to the XPS equipment after cleaning with deionized water and dried in air. XPS test was performed using a monochromatic Al Kα x-ray source. The software Xpspeak version 4.1 with a Shirley

background subtraction was used to fit the data. The standard C1s peak (284.8 eV) was chosen as the calibration peak.

3. Results and Discussion

3.1 Polarization Curves Measured at Various Cl^- Concentrations

Figure 2 shows the polarization curves of 2507 SDSS in saturated $Ca(OH)_2$ solution containing different chloride concentrations. Clearly, all curves display the passivation characteristics. With the increase of Cl^- concentration, the curve shifts rightward, and the corrosion potential of 2507 SDSS shifts negatively when Cl^- ions are added to saturated $Ca(OH)_2$ solution. This suggests that the addition of Cl^- ions enhances the corrosion trends. The fitted passive current density (i_p) is shown in Fig. 3. In the absence of chloride ions, the i_p value is the lowest. In contrast, the presence of chloride ions increases the i_p value, especially at the concentration of 10%. This indicates that Cl^- ions accelerate the corrosion of SDSS in the saturated $Ca(OH)_2$ solution, which may be attributed to Cl^- ions destroying the passive film formed on the SDSS surface. In other words, Cl^- ions reduce the protective ability of passive film, causing an increase in the corrosion rate of SDSS.

3.2 Electrochemical Curves Measured at Various AC Current Densities

Figure 4 shows the polarization curves of 2507 SDSS at various AC current densities in saturated $Ca(OH)_2$ solution with 3.5% Cl^-. Similarly, the SDSS sample applied at different AC current densities (i_{AC}) exhibits the apparent passivation behavior. However, the imposed AC affects the passivation characteristics, narrowing the passive region. The anode branch visibly shifts to the right upon applying a small i_{AC} of 30 A/m^2. The fitted i_p and (critical pitting potential) E_p are revealed in Fig. 5. As the applied i_{AC} increases, the i_p value increases, and the E_p value decreases, especially at the high i_{AC}. When i_{AC} is increased up to 200 A/m^2, the i_p increases more than three times as much as that of SDSS without AC interference, and the E_p drops from 0.536 to 0.132 V_{SCE}. This clearly indicates that the imposed AC significantly reduces the passivity of SDSS and promotes the pitting corrosion sensitivity.

To further explore the destructive influence of applied AC on the passive film formed on the surface of SDSS specimen using potentiostatic polarization method, the EIS diagram and Mott-Schottky curves were measured.

Figure 6 shows the impedance spectra of 2507 SDSS interfered at different AC current densities for 5 min in saturated $Ca(OH)_2$ solution with 3.5% Cl^-. All curves display the feature of capacitive reactance arc. With the increase of i_{AC}, the diameter of semi-circle arc decreases, especially at high i_{AC} of 100 A/m^2 and 200 A/m^2. In the absence of AC interference, the diagram exhibits the largest arc diameter, the highest phase angle in medium frequency region and the maximal impedance value in the low-frequency of 10 mHz. These characteristics demonstrate that the passive film without AC application has the optimal protective ability (Ref 38, 39). When AC is applied,

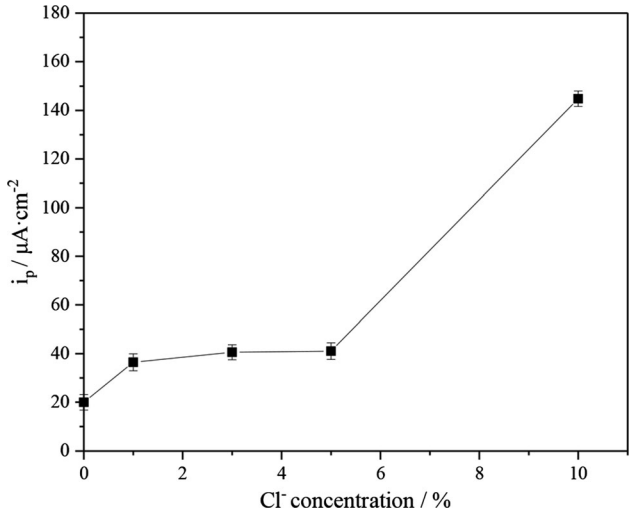

Fig. 3 Passive current density (i_p) of 2507 SDSS in chloride-containing saturated $Ca(OH)_2$ solution with various Cl^- concentrations

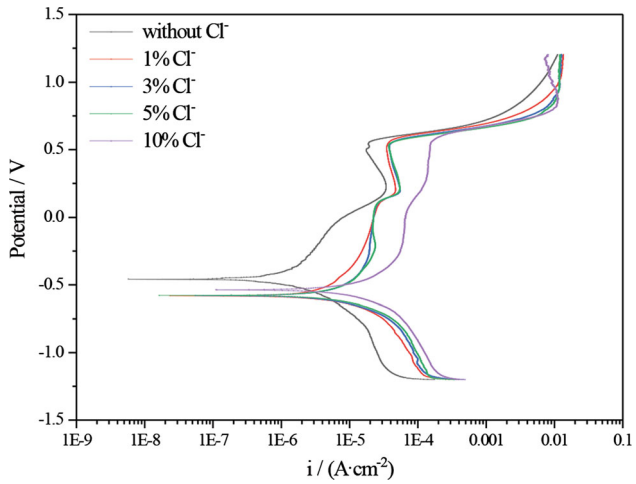

Fig. 2 Polarization curves of 2507 SDSS in chloride-containing saturated $Ca(OH)_2$ solution with various Cl^- concentrations

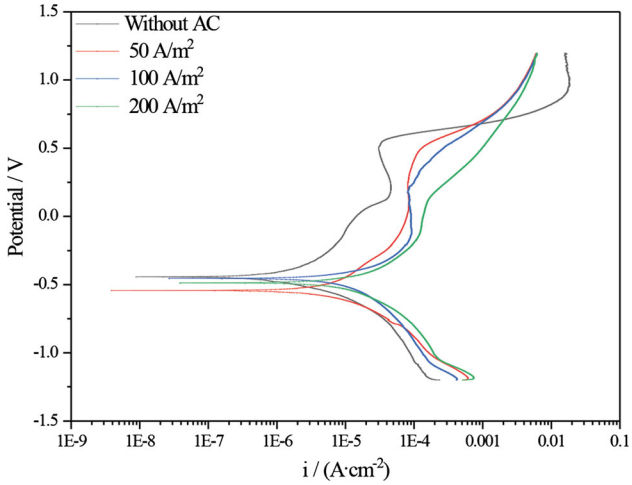

Fig. 4 Polarization curves of 2507 SDSS at various AC current densities in saturated $Ca(OH)_2$ solution with 3.5% Cl^-

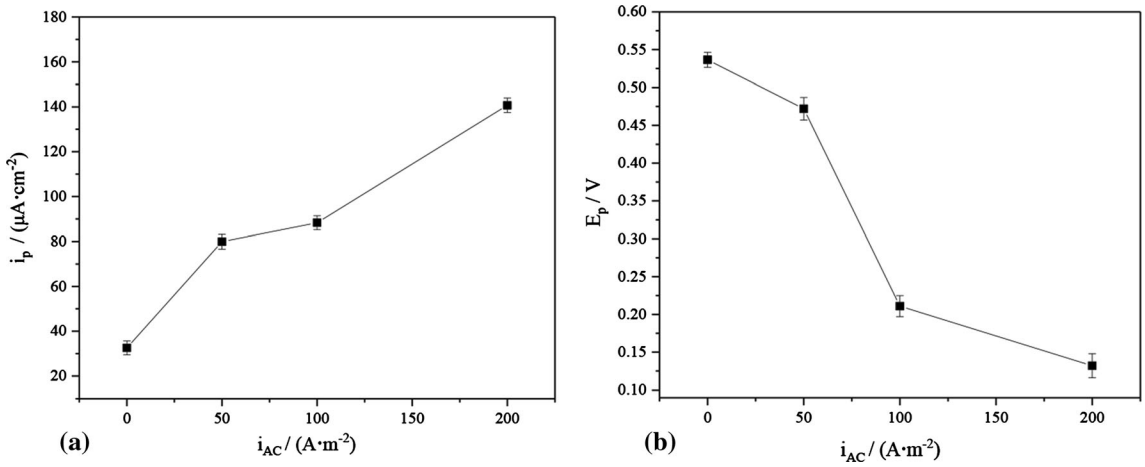

Fig. 5 Fitted corrosion parameters of 2507 SDSS at various AC current densities in saturated $Ca(OH)_2$ solution with 3.5% Cl^-. (a) i_p; (b) E_p

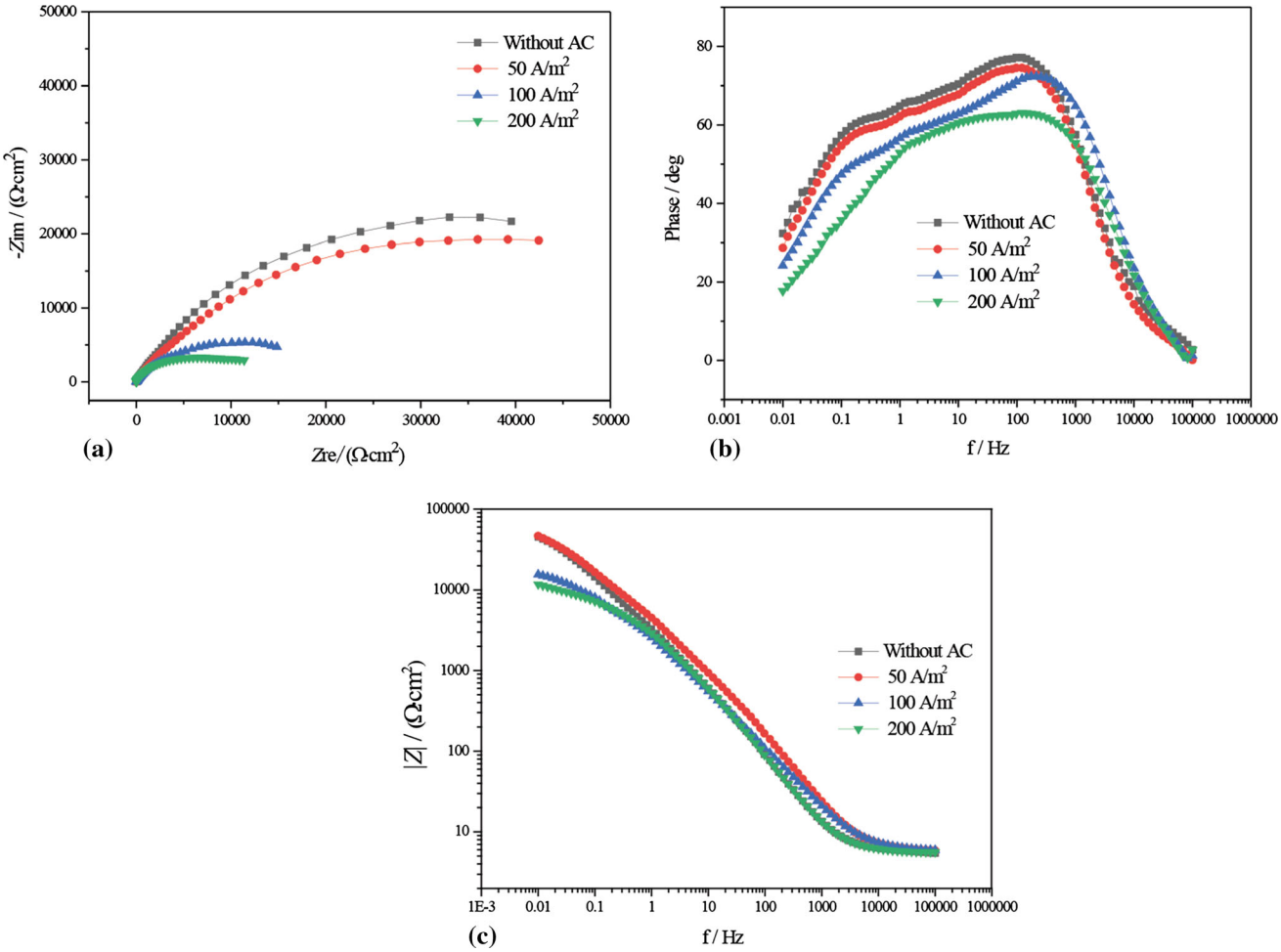

Fig. 6 Impedance spectra of 2507 SDSS interfered at different AC current densities for 5 min in saturated $Ca(OH)_2$ solution with 3.5% Cl^-; (a) Nyquist plots; (b) Bode plots

the sharp decrease in these parameters indicates that imposed AC decreases the anti-corrosion property of passive film.

An equivalent circuit was used to fit the EIS data (Fig. 7), where R_s is the solution resistance, Q_f denotes the capacitance of passive film, R_f represents the resistance of passive film. Q_{dl} corresponds to the double-layer capacitance at the matrix/solution interface and R_{ct} is the charge transfer resistance. Table 1 lists the fitted electrochemical parameters. As the i_{AC} increases, the R_f and R_{ct} values decrease. The SDSS sample without AC interference exhibits the highest R_f value, indicating that the passive film is relatively compact. R_{ct} reveals the degree of difficulty for charge to reach the electrode substrate interface

through the electrolyte solution and the surface passive film (Ref 40-42). The largest R_{ct} value demonstrates that the dense film possesses the best corrosion resistance. In the presence of imposed AC, the marked decrease in R_f means that a decrease in the resistance to charge and species migration in the passive film, causing the film to be unstable and weakening the protective ability of SDSS. Similar variation trend in the R_{ct} value confirms that AC interference results in a harmful effect on the passive film. The higher the i_{AC}, the more severe the damage influence is.

To further analyze the destructive influence of superimposed AC on passive film, the Mott–Schottky measurement was adopted to investigate the structural change within the passive film. The relationship between space charge capacitance (C) and applied potential can be given by the Mott–Schottky Eq 1 and 2:

$$\frac{1}{C^2} = \frac{2}{\varepsilon\varepsilon_0 e N_D}\left(E - E_{fb} - \frac{kT}{e}\right), \quad \text{for } n\text{-type semiconductors} \tag{Eq 1}$$

$$\frac{1}{C^2} = -\frac{2}{\varepsilon\varepsilon_0 e N_A}\left(E - E_{fb} - \frac{kT}{e}\right), \quad \text{for } p\text{-type semiconductors} \tag{Eq 2}$$

where N_D and N_A denote the donor and acceptor densities (cm^{-3}), respectively, e is the electron charge (1.602189×10^{-19} C), ε is the relative dielectric constant of the passive film, ε_0 is the permittivity of the vacuum (8.854×10^{-12} F m^{-1}), T is the Kelvin temperature, k is Boltzmann's constant (1.38×10^{-23} J K^{-1}), E is the applied electrode potential (V vs. SCE), and E_{fb} represents the flat band potential (V vs. SCE). N_D and N_A can be calculated from the slopes of the linear portion of Mott–Schottky curves.

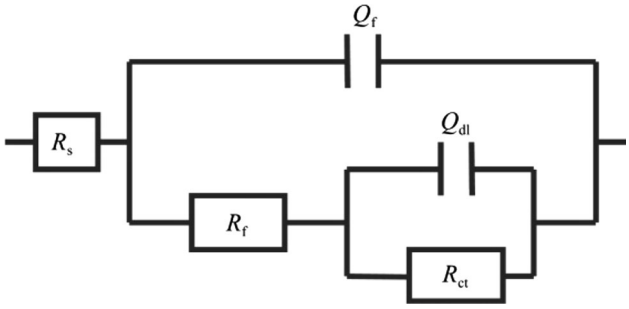

Fig. 7 Equivalent circuit for fitting EIS data

Figure 8 shows the Mott–Schottky curves of 2507 SDSS interfered at different AC current densities for 5 min in saturated $Ca(OH)_2$ solution with 3.5% Cl^-. Obviously, a significant difference in the curve characteristics is observed. It is well known that the positive and negative slopes of linear segments denote n-type and p-type semiconductor behavior, respectively. Hence, in the potential range of − 1.0 to 1.0 V, the passive film without AC application exhibits the semiconductor behavior of n-p-n-p, whereas the film interfered at different AC current densities reveals the n-p type semiconductor feature. This indicates that the applied AC affects the electronic property of the surface film. Figure 9 exhibits the calculated N_D and N_A values. As the AC current density increases, the two parameter values gradually increase. Especially at the high AC current density of 200 A/m^2, a marked increase can be seen. This means that AC interference increases the number of defects within the passive film (Ref 25). This may be attributed to that AC interference can promote the migration rate of ions (e.g., Cl^-), in this case, more Cl^- ions can absorb on the film surface. The Cl^- ions react with oxygen vacancies to form the cationic vacancies, generating a harmful influence on the passive film. The existence of defects can reduce the compactness and stability of the film, decrease the diffusion resistance of species and charge, and promote the rate of electrochemical reaction. Therefore, the minimum N_D and N_A values reveal that the film without applied AC is relatively dense, thereby offering the best protective ability. Whereas the film with AC interference contains a great number of defects and causes a decrease in the anti-corrosion resistance.

3.3 Immersion Test

Figure 10 shows the corrosion rate of 2507 SDSS immersed in the saturated $Ca(OH)_2$ solution with 3.5% Cl^- at different AC current densities for 10 d. As i_{AC} increases, the corrosion rate of SDSS increases. In the absence of applied AC, the corrosion rate is the lowest. When a low i_{AC} of 50A/m^2 is applied, the corrosion rate increases up to more than twice of that without AC application. Whereas a sharp increase trend is exhibited at the high i_{AC} of 100 A/m^2. The corrosion morphologies of SDSS shown in Fig. 11 demonstrate the difference in corrosion resistance in detail. Without applied AC, the SDSS sample exhibits a slight corrosion degree, with sporadic pits. In the presence of AC, the number of pits apparently increases. The results demonstrate that AC damages the surface film, decreasing the passivity and protective ability of SDSS.

It is generally accepted that the composition of passive film is one of the key factors that can greatly affect the corrosion

Table 1 Fitted electrochemical parameters for EIS data of 2507 SDSS at various AC current densities in saturated $Ca(OH)_2$ solution with 3.5% Cl^-

i_{AC}, A/m^2	R_s, Ω cm^2	Q_f, 10^{-5} Ω^{-1} cm^{-2} s^n	n_f	R_f, Ω cm^2	Q_{dl}, 10^{-5} Ω^{-1} cm^{-2} s^n	n_{dl}	R_{ct}, 10^4 Ω cm^2
0	5.617	8.663	0.7711	1690	7.671	0.814	8.0860
50	5.566	8.266	0.8566	1470	7.783	0.8405	7.1740
100	5.654	5.162	0.875	348.8	8.116	0.8004	1.1763
200	5.256	4.537	0.8319	307.6	8.291	0.8919	0.8987

n_f and n_{dl} are phenomenological coefficients

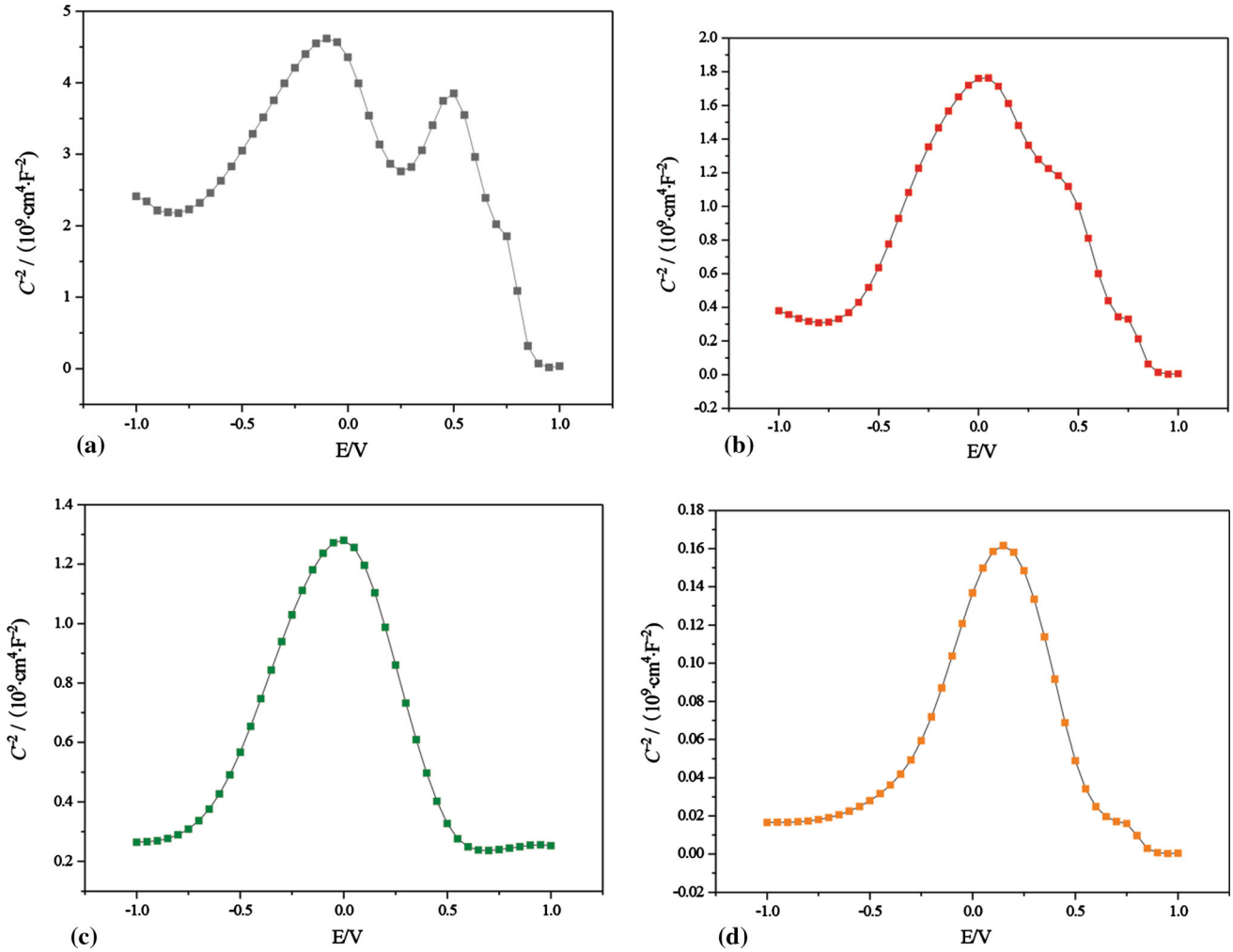

Fig. 8 Mott–Schottky curves of 2507 SDSS interfered at different AC current densities for 5 min in saturated $Ca(OH)_2$ solution with 3.5% Cl^-. (a) without AC (b) 50A/m^2 (c) 100 A/m^2 (d) 200 A/m^2

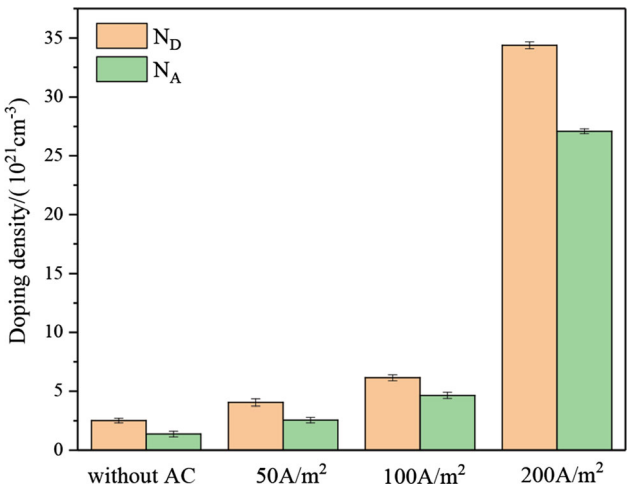

Fig. 9 Calculated N_D and N_A values of passive films of 2507 SDSS interfered at different AC current densities for 5 min in saturated $Ca(OH)_2$ solution with 3.5% Cl^-

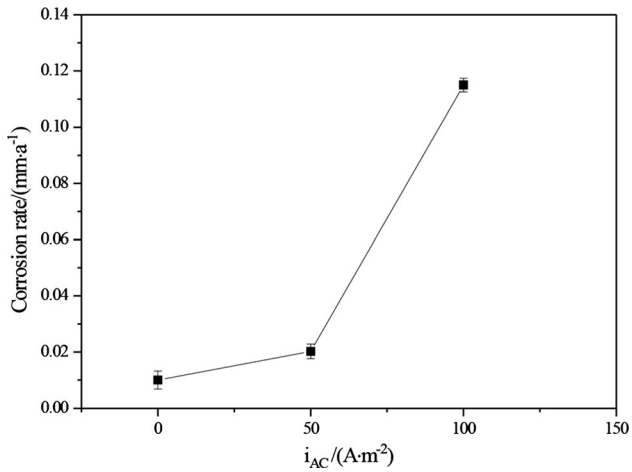

Fig. 10 Corrosion rate of 2507 SDSS immersed in saturated $Ca(OH)_2$ solution with 3.5% Cl^- under different AC current densities for 10d

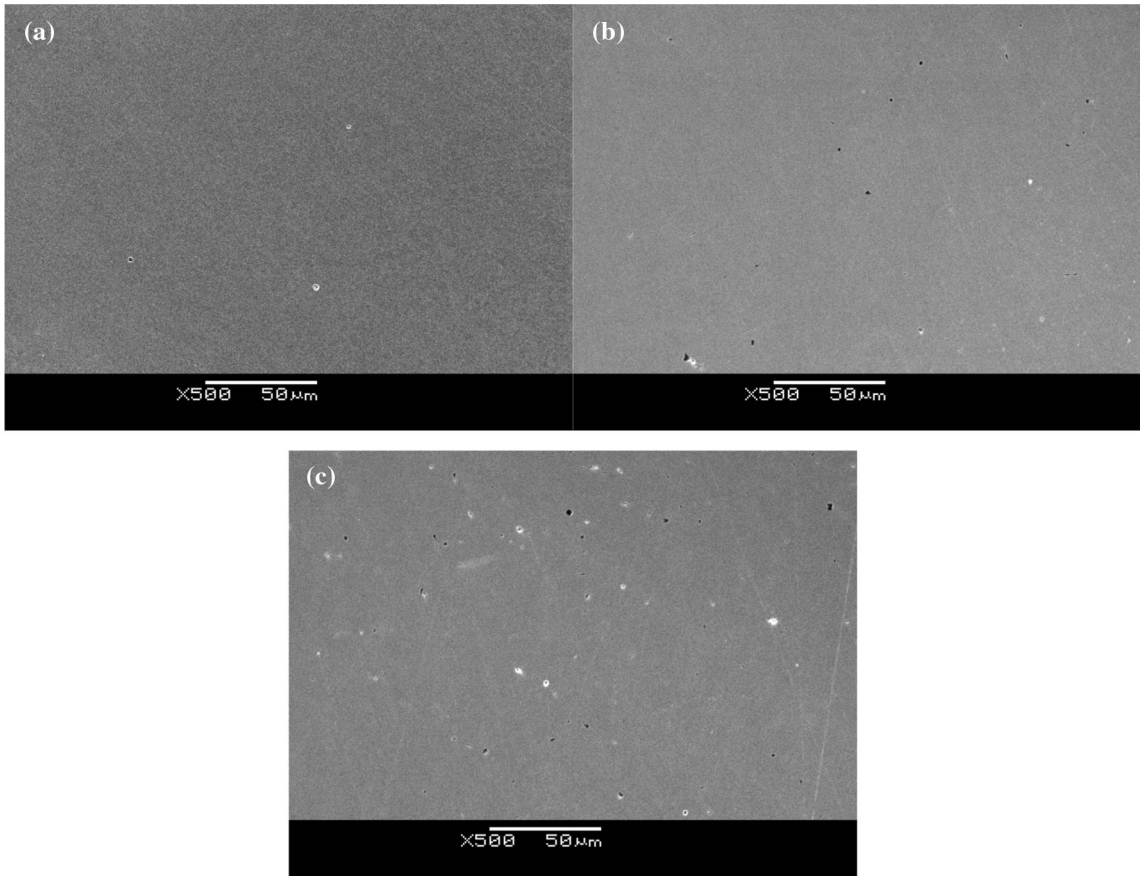

Fig. 11 Corrosion morphologies of 2507 SDSS immersed in saturated $Ca(OH)_2$ solution with 3.5% Cl^- under different AC current densities for 10d. (a) without AC (b)50A/m^2 (c)100 A/m^2

resistance of SDSS; thus, we adopted the XPS measurement to investigate the change in the composition of the passive film interfered with and without the imposed AC in this work.

3.4 XPS Analysis of Passive Film

Figure 12 shows the XPS fitting results of Cr2$p_{3/2}$ of the passive film formed on 2507 SDSS under three testing conditions. Cr mainly exists in the form of Cr_2O_3 and $Cr(OH)_3$. Cr_2O_3 is the primary constituent of the passive film formed in the saturated $Ca(OH)_2$ solution. It is generally believed that the presence of Cr_2O_3 is conducive to enhancing the corrosion resistance of passive film (Ref 43). Therefore, the film formed under this condition possesses the noble anti-corrosion property. After the addition of 3.5% NaCl to the saturated $Ca(OH)_2$ solution, the intensity of $Cr(OH)_3$ peak increases, indicating that the existence of Cl^- reduces the protective ability of the film (Ref 44). When 100 A/m^2 is applied, the intensity of $Cr(OH)_3$ peak becomes higher, whereas the intensity of Cr_2O_3 peak decreases significantly, which implies that the addition of 3.5% NaCl and the application of AC generate a combined effect, significantly decreasing the corrosion resistance of passive film.

The detailed XPS spectra of Fe 2$p_{3/2}$ of passive film formed on 2507 SDSS under three testing conditions are depicted in Fig. 13. The passive film is mainly composed of two constituents of Fe_2O_3 and $Fe(OH)_3$. The ratio of Fe_2O_3 and $Fe(OH)_3$ in the passive film formed in the saturated $Ca(OH)_2$ solution is close to 1:1. Nevertheless, both the addition of 3.5% NaCl and the application of AC can decrease the intensity of $Fe(OH)_3$ peak.

As shown in Fig. 14, the spectra of O1*s* are split into three peaks: O^{2-}, OH^-, and H_2O. OH^- is the primary constituent of passive film formed in the saturated $Ca(OH)_2$ solution. The intensity of O^{2-} peak increases when 3.5% NaCl is added to saturated $Ca(OH)_2$ solution. Furthermore, the peak intensity of bound water of the film formed in the saturated $Ca(OH)_2$ solution containing 3.5% NaCl decreases obviously after AC interference, which suggests that the stability and anti-corrosion property of passive film further decreases (Ref 45, 46). The above change in the constituent of passive film causes an evolution in its electronic property (Ref 47, 48). The binding energies of primary compounds acquired from the XPS spectral deconvolution were referenced to the literature (Ref 49, 50).

In summary, it can be found that the applied AC and the addition of Cl^- exert a synergistic effect, reducing the corrosion resistance of passive film formed on 2507 SDSS.

4. Conclusions

The presence of Cl^- ions accelerates the corrosion of 2507 SDSS in the saturated $Ca(OH)_2$ solution. The protective ability of passive film decreases as Cl^- concentration increases, especially at the concentration of 10% Cl^-. As the applied i_{AC}

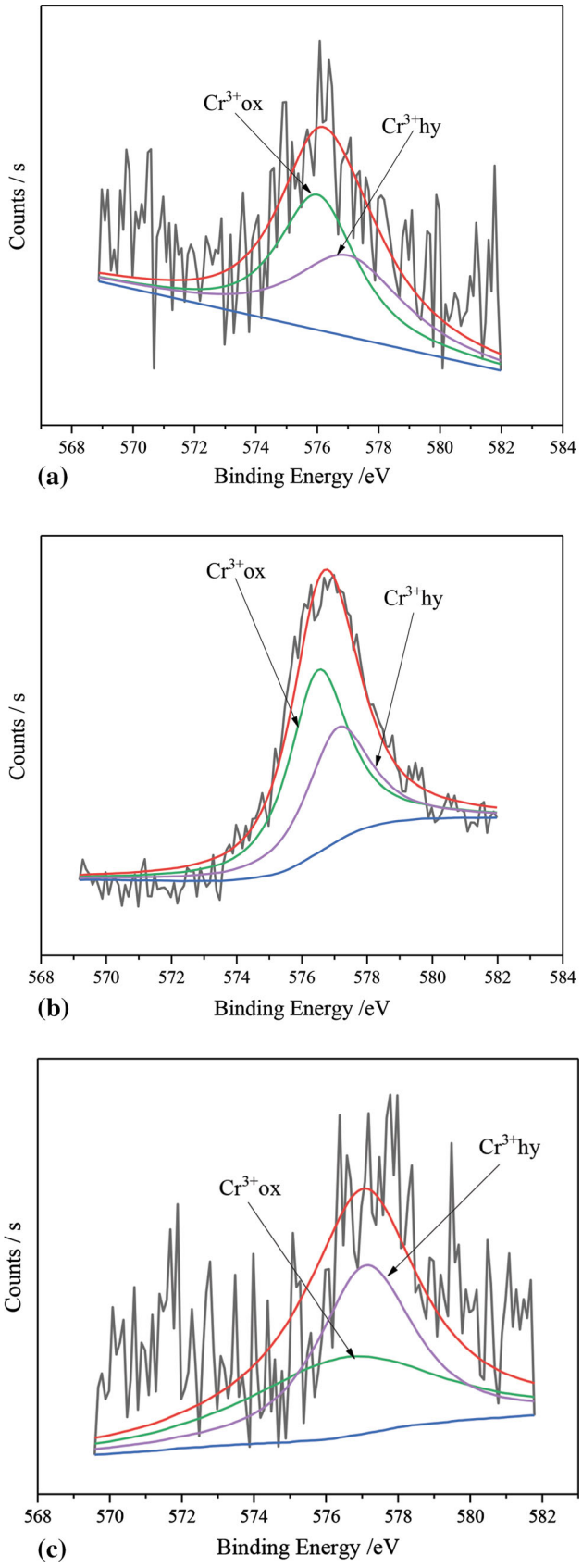

Fig. 12 The XPS spectra of Cr $2p_{3/2}$ of the passive films formed on 2507 SDSS in saturated $Ca(OH)_2$ solution measured under three conditions. (a) without Cl^- (b) with the addition of 3.5% Cl^- (c) combined action of 3.5% Cl^- and i_{AC} of 100 A/m^2

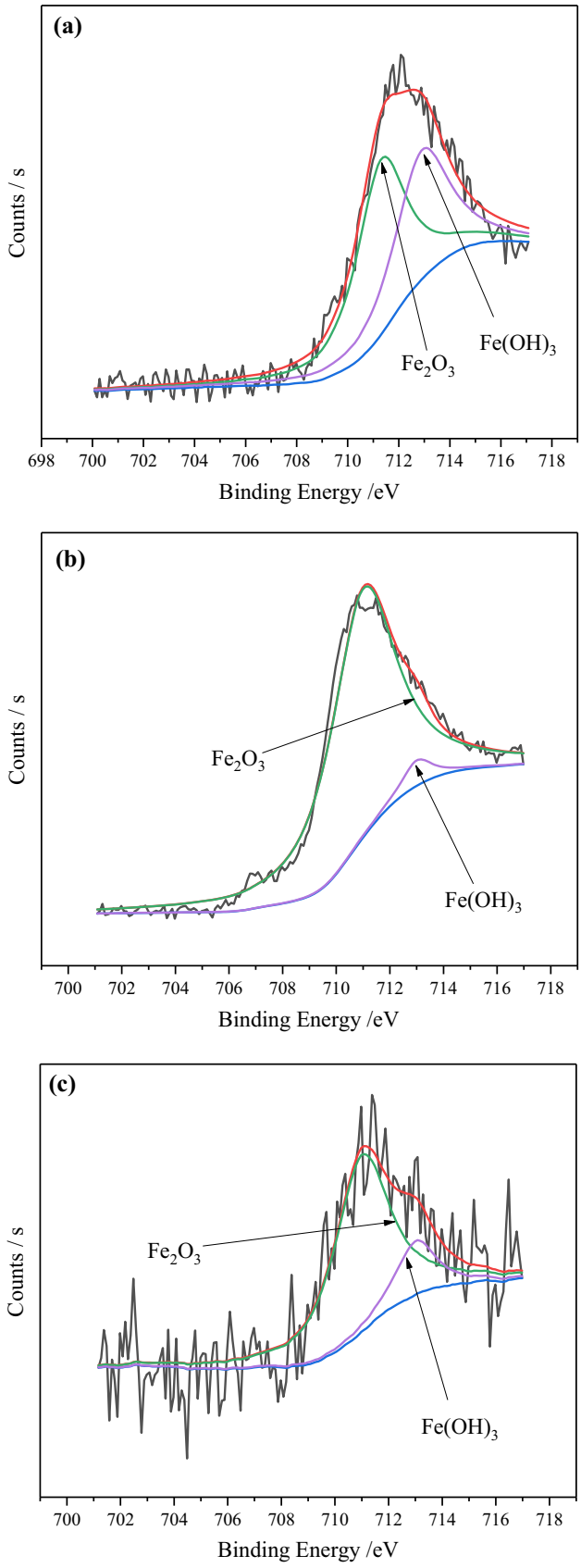

Fig. 13 The XPS spectra of Fe $2p_{3/2}$ of the passive films formed on 2507 SDSS in saturated $Ca(OH)_2$ solution measured under three conditions (a) without Cl^- (b) with the addition of 3.5% Cl^- (c) combined action of 3.5% Cl^- and i_{AC} of 100 A/m ^{2}

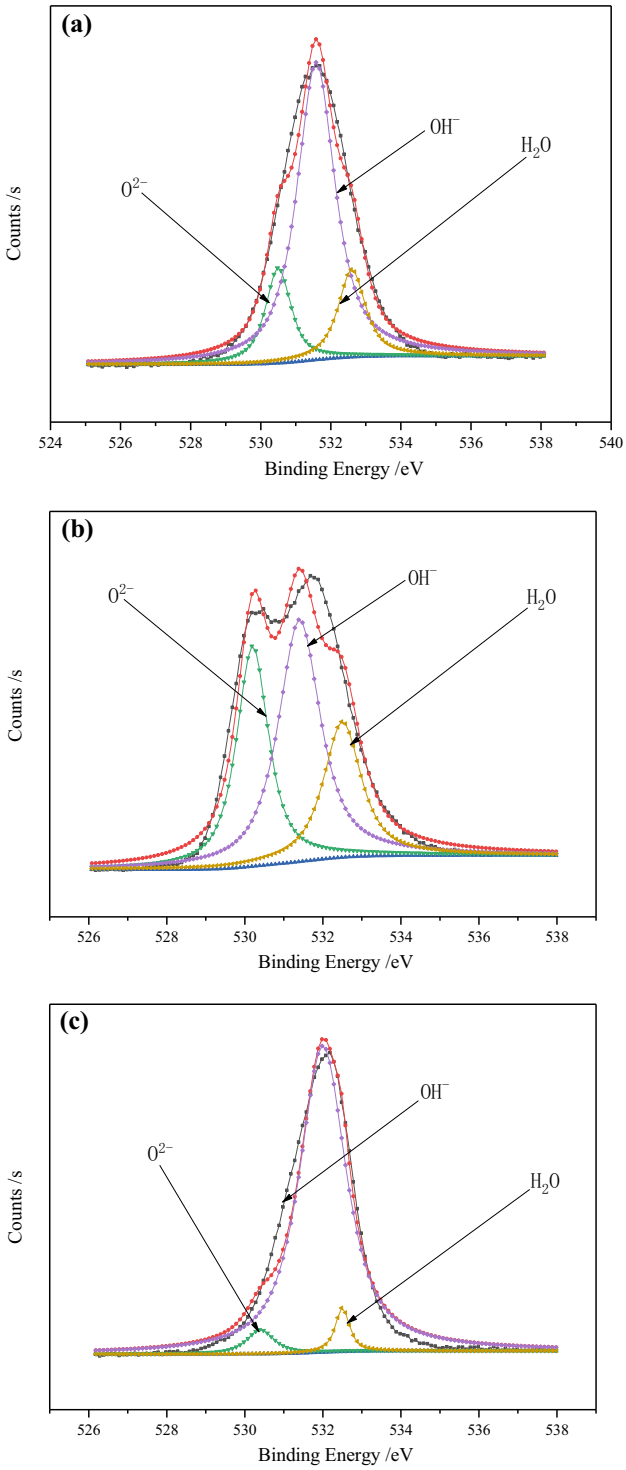

Fig. 14 The XPS spectra of O1*s* of the passive films formed on 2507 SDSS in saturated $Ca(OH)_2$ solution measured under three conditions. (a) without Cl^- (b) with the addition of 3.5% Cl^- (c) combined action of 3.5% Cl^- and i_{AC} of 100 A/m^2

increases, the i_p value increases, and the E_p value decreases. The applied AC increases the number of defects within the passive film, affects the electronic property of the surface film, which results in a harmful effect on the passive film, and weakens its anti-corrosion property. The higher the i_{AC}, the more severe the damage influence is. Moreover, imposed AC promotes the pitting corrosion sensitivity of SDSS, and enhances its corrosion rate. The addition of Cl^- and the application of AC generate a combined effect, significantly decreasing the corrosion resistance of passive film.

Acknowledgments

This work was supported by the Natural Science Foundation of Zhejiang Province of China (No. LY18E010004) and National Material Environmental Corrosion Infrastructure.

References

1. K.K. Tang, Stray Alternating Current (AC) Induced Corrosion of Steel Fibre Reinforce Concrete, *Corros. Sci.*, 2019, **152**, p 153–171
2. A. Brenna, S. Beretta, F. Bolzoni, M.P. Pedeferri, and M. Ormellese, Effects of AC-Interference on Chloride-Induced Corrosion of Reinforced Concrete, *Constr. Build. Mater.*, 2017, **137**, p 76–84
3. M. Zhu, Q. Zhang, Y.F. Yuan, S.Y. Guo, and Y.B. Chen, Study on the Microstructure and Alternating Current Corrosion Behavior of SAF2507 Super-Duplex Stainless Steel in 3.5%NaCl Solution, *J. Mater. Eng. Perform.*, 2020, **29**, p 1366–1374
4. Z.T. Jiang, Y.X. Du, L. Dong, and M.X. Lu, Effect of AC Current on Corrosion Potential of Q235 Steel, *Acta Metall. Sin.*, 2011, **47**, p 997–1002
5. D.Z. Tang, Y.X. Du, X.X. Li, Y. Liang, and M.X. Lu, Effect of Alternating Current on the Performance of Magnesium Sacrificial Anode, *Mater. Des.*, 2016, **93**, p 133–145
6. A.Q. Fu and Y.F. Cheng, Effects of Alternating Current on Corrosion of a Coated Pipeline Steel in a Chloride-Containing Carbonate/Bicarbonate Solution, *Corros. Sci.*, 2010, **52**, p 612–619
7. C. Wen, J. Li, S. Wang, and Y. Yang, Experimental Study on Stray Current Corrosion of Coated Pipeline Steel, *J. Nat. Gas Sci. Eng.*, 2015, **27**, p 1555–1561
8. H.X. Wan, D.D. Song, C.W. Du, Z.Y. Liu, and X.G. Li, Effect of Alternating Current and Bacillus Cereus on the Stress Corrosion Behavior and Mechanism of X80 Steel in a Beijing Soil Solution, *Bioelectrochemistry*, 2019, **127**, p 49–58
9. L.W. Wang, L.J. Cheng, J.R. Li, Z.F. Zhu, S.W. Bai, and Z.Y. Cui, Combined Effect of Alternating Current Interference and Cathodic Protection on Pitting Corrosion and Stress Corrosion Cracking Behavior of X70 Pipeline Steel in Near-Neutral pH Environment, *Materials*, 2018, **11**, p 465–483
10. M. Zhu, C.W. Du, X.G. Li, Z.Y. Liu, H. Li, and D.W. Zhang, Effect of AC on Stress Corrosion Cracking Behavior and Mechanism of X80 Pipeline Steel in Carbonate/Bicarbonate Solution, *Corros. Sci.*, 2014, **87**, p 224–232
11. M. Zhu, Y.F. Yuan, S.M. Yin, G.H. Yu, S.Y. Guo, Y.Z. Huang, and C.W. Du, Corrosion Behavior of Pipeline Steel with Different Microstructures Under AC Interference in Acid Soil Simulation Solution, *J. Mater. Eng. Perform.*, 2019, **28**, p 1698–1706
12. M. Zhu, J. Ma, Y.F. Yuan, S.Y. Guo, S.M. Yin, and C.W. Du, The Effect of Annealing Time on Microstructure and AC Corrosion Behavior of X80 Steel in Simulated Solution of Alkaline Soil, *J. Mater. Eng. Perform.*, 2019, **28**, p 6073–6080
13. M. Zhu, J.L. Yang, Y.B. Chen, Y.F. Yuan, and S.Y. Guo, Effect of Alternating Current on Passive Film and Corrosion Behavior of Pipeline Steel with Different Microstructures in Carbonate/Bicarbonate Solution, *J. Mater. Eng. Perform.*, 2020, **29**, p 423–433
14. Q. Liu, W. Wu, Y. Pan, Z.Y. Liu, and X.G. Li, Electrochemical Mechanism of Stress Corrosion Cracking of API, X70 Pipeline Steel under Different AC Frequencies, *Constr. Build. Mater.*, 2018, **171**, p 622–633
15. Y.B. Guo, T. Meng, D.G. Wang, H. Tan, and R.Y. He, Experimental Research on the Corrosion of X Series Pipeline Steels under Alternating Current Interference, *Eng. Fail. Anal.*, 2017, **78**, p 87–98
16. J.L. Wendt and D.T. Chin, The AC Corrosion of Stainless Steel-II. The Breakdown of Passivity of SS304 in Neutral Aqueous Solutions, *Corros. Sci.*, 1985, **25**, p 889–900

17. I. Calderon-Uriszar-Aldaca, E. Briz, P. Larrinaga, and H. Garcia, Bonding Strength of Stainless Steel Rebars in Concretes Exposed to Marine Environments, *Constr. Build. Mater.*, 2018, **172**, p 125–133
18. E.Z. Zhou, H.B. Li, C.T. Yang, J.J. Wang, and T.Y. Gu, Accelerated Corrosion of 2304 Duplex Stainless Steel by Marine Pseudomonas Aeruginosa Biofilm, *Int. Biodeter. Biodegr.*, 2018, **127**, p 1–9
19. H. Tan, Z.Y. Wang, Y.M. Jiang, D. Han, J.F. Hong, L.D. Chen, L.Z. Jiang, and J. Lin, Annealing Temperature Effect on the Pitting Corrosion Resistance of Plasma Arc Welded Joints of Duplex Stainless Steel UNS S32304 in 1.0 M NaCl, *Corros. Sci.*, 2011, **53**, p 2191–2200
20. L. Bertolini, F. Bolzoni, T. Pastore, and P. Pedeferri, Behaviour of Stainless Steel in Simulated Concrete Pore Solution, *Br. Corros. J.*, 1996, **31**, p 218–222
21. A. Bautista, G. Blanco, F. Velasco, A. Gutierrez, S. Palacin, L. Soriano, and H. Takenouti, Passivation of Duplex Stainless Steels in Solutions Simulating Chloride-Contaminated Concrete, *Mater. Construct.*, 2007, **57**, p 17–31
22. A. Bautista, G. Blanco, F. Velasco, and M.A. Martínez, Corrosion Performance of Welded Stainless Steels Reinforcements in Simulated Pore Solutions, *Constr. Build. Mater.*, 2007, **21**, p 1267–1276
23. L. Veleva, A.A. Alpuche-Avilés, M.K. Graves-Brook, and D.O. Wipf, Comparative Cyclic Voltammetry and Surface Analysis of Passive Films Grown on Stainless Steel 316 in Concrete Pore Model Solutions, *J. Electroanal. Chem.*, 2005, **538**, p 45–53
24. Y. Wu and U. Nürnberger, Corrosion-Technical Properties of High-Strength Stainless Steels for the Application in Prestressed Concrete Structures, *Mater. Corros.*, 2009, **60**, p 771–780
25. H. Luo, H.Z. Su, C.F. Dong, and X.G. Li, Passivation and Electrochemical Behavior of 316L Stainless Steel in Chlorinated Simulated Concrete Pore Solution, *Appl. Surf. Sci.*, 2017, **400**, p 38–48
26. M.C. Alonso, F.J. Luna, and M. Criado, Corrosion Behavior of Duplex Stainless Steel Reinforcement in Ternary Binder Concrete Exposed to Natural Chloride Penetration, *Constr. Build. Mater.*, 2019, **199**, p 385–395
27. E. Briz, M.V. Biezma, and D.M. Bastidas, Stress Corrosion Cracking of New 2001 Lean-Duplex Stainless Steel Reinforcements in Chloride Contained Concrete Pore Solution: An Electrochemical Study, *Constr. Build. Mater.*, 2018, **192**, p 1–8
28. R.D. Moser, P.M. Singh, L.F. Kahn, K.E. Kurtis, and Z.B. McClelland, Crevice Corrosion and Environmentally Assisted Cracking of High-Strength Duplex Stainless Steels in Simulated Concrete Pore Solutions, *Constr. Build. Mater.*, 2019, **203**, p 366–376
29. M. Chen, H.B. Liu, L.B. Wang, C.X. Wang, and V. Ji, Evaluation of the Residual Stress and Microstructure Character in SAF 2507 Duplex Stainless Steel after Multiple Shot Peening Process, *Surf. Coat. Tech.*, 2018, **344**, p 132–140
30. Z.Y. Zhang, H.Z. Zhang, J. Hu, X.X. Qi, and Y.Q. Zhao, Microstructure Evolution and Mechanical Properties of Briefly Heat-Treated SAF 2507 Super Duplex Stainless Steel Welds, *Constr. Build. Mater.*, 2018, **168**, p 338–345
31. Z.Y. Cui, L.W. Wang, H.T. Ni, W.K. Hao, and X.G. Li, Influence of Temperature on the Electrochemical and Passivation Behavior of 2507 Super Duplex Stainless Steel in Simulated Desulfurized Flue Gas Condensates, *Corros. Sci.*, 2018, **168**, p 338–345
32. N.W. Dai, J. Wu, L.C. Zhang, Y.T. Sun, Y.Y. Liu, Y.Y. Yang, Y.M. Jiang, and J. Li, Alternating Voltage Induced Oscillation on Electrochemical Behavior and Pitting Corrosion in Duplex Stainless Steel 2205, *Mater. Corros.*, 2019, **70**, p 419–433
33. D.K. Kim, S.V. Muralidharan, T.H. Ha, J.H. Bae, Y.C. Ha, H.G. Lee, and J.D. Scantlebury, Electrochemical Studies on the Alternating Current Corrosion of Mild Steel under Cathodic Protection Condition in Marine Environments, *Electrochim. Acta*, 2006, **51**, p 5259–5267
34. M. Liu, X. Cheng, X. Li, Z. Jin, and H. Liu, Corrosion Behavior of Cr Modified HRB400 Steel Rebar in Simulated Concrete Pore Solution, *Constr. Build. Mater.*, 2015, **93**, p 884–890
35. E.C. Paredes, A. Bautista, S.M. Alvarez, and F. Velasco, Influence of the Forming Process of Corrugated Stainless Steels on their Corrosion Behaviour in Simulated Pore Solutions, *Corros. Sci.*, 2012, **58**, p 52–61
36. S. Fajardo, D.M. Bastidas, M.P. Ryan, M. Criado, and J.M. Bastidas, Low-Nickel Stainless Steel Passive Film in Simulated Concrete Pore Solution: A SIMS Study, *Appl. Surf. Sci.*, 2010, **256**, p 6139–6143
37. M. Zhu, C.W. Du, X.G. Li, Z.Y. Liu, S.R. Wang, J.K. Li, and D.W. Zhang, Effect of AC Current Density on Stress Corrosion Cracking Behavior of X80 Pipeline Steel in High pH Carbonate/Bicarbonate Solution, *Electrochim. Acta*, 2014, **117**, p 351–359
38. B. Díaz, B. Guitián, X.R. Nóvoa, and M.C. Pérez, The Effect of Long-Term Atmospheric Aging and Temperature on the Electrochemical Behaviour of Steel Rebars in Mortar, *Corros. Sci.*, 2018, **140**, p 143–150
39. R.G. Duarte, A.S. Castela, R. Neves, L. Freire, and M.F. Montemor, Corrosion Behavior of Stainless Steel Rebars Embedded in Concrete: An Electrochemical Impedance Spectroscopy Study, *Electrochim. Acta*, 2014, **124**, p 218–224
40. M. Liu, X.Q. Cheng, X.G. Li, and T.J. Lu, Corrosion Behavior of Low-Cr Steel Rebars in Alkaline Solutions with Different pH in the Presence of Chlorides, *J. Electroanal. Chem.*, 2017, **803**, p 40–50
41. M. Liu, X.Q. Cheng, X.G. Li, Y. Pan, and J. Li, Effect of Cr on the Passive Film Formation Mechanism of Steel Rebar in Simulated Concrete Pore Solution, *Appl. Surf. Sci.*, 2016, **389**, p 1182–1191
42. M. Liu, X.Q. Cheng, X.G. Li, C. Zhou, and H.L. Tan, Effect of Carbonization on the Electrochemical Behavior of Corrosion Resistance Low Alloy Steel Rebars in Cement Extract Solution, *Constr. Build. Mater.*, 2017, **130**, p 193–201
43. Z.Y. Cui, L.W. Wang, H.T. Ni, W.K. Hao, and X.G. Li, Influence of Temperature on the Electrochemical and Passive Behavior of 2507 Super Duplex Stainless Steel in Simulated Desulfurized Flue Gas Condensates, *Corros. Sci.*, 2017, **118**, p 31–48
44. C. Clayton and Y. Lu, A Bipolar Model of the Passivity of Stainless Steel: the Role of Mo Addition, *J. Electrochem. Soc.*, 1986, **133**, p 2465–2473
45. G. Okamoto and T. Shibata, Desorption of Tritiated Bound-Water from the Passive Film Formed on Stainless Steels, *Nature*, 1965, **206**, p 1350
46. K. Hashimoto, K. Asami, and K. Teramoto, An X-Ray Photo-Electron Spectroscopic Study on the Role of Molybdenum in Increasing the Corrosion Resistance of Ferritic Stainless Steels in HC1, *Corros. Sci.*, 1979, **19**, p 3–14
47. H. Luo, C.F. Dong, K. Xiao, and X.G. Li, Characterization of Passive Film on 2205 Duplex Stainless Steel in Sodium Thiosulphate Solution, *Appl. Surf. Sci.*, 2011, **258**, p 631–639
48. R.M. Fernández-Domene, E. Blasco-Tamarit, D.M. García-García, and J. García-Antón, Passive and Transpassive Behaviour of Alloy 31 in a Heavy Brine LiBr Solution, *Electrochim. Acta*, 2013, **95**, p 1–11
49. L.W. Wang, H.Y. Tian, H. Gao, F.Z. Xie, K. Zhao, and Z.Y. Cui, Electrochemical and XPS Analytical Investigation of the Accelerative Effect of Bicarbonate/Carbonate Ions on AISI, 304 in Alkaline Environment, *Appl. Surf. Sci.*, 2019, **492**, p 792–807
50. Z.Y. Cui, S.S. Chen, L.W. Wang, C. Man, Z.Y. Liu, J.S. Wu, X. Wang, S.G. Chen, and X.G. Li, Passivation Behavior and Surface Chemistry of 2507 Super Duplex Stainless Steel in Acidified Artificial Seawater Containing Thiosulfate, *J. Electrochem. Soc.*, 2017, **164**, p C856–C868